Dental Research Journal

Original Article

The influence of internally architected voids in the creation of high-strength, low-weight 3D-printed cobalt–chromium prototypes

Abdullah Jasim Mohammed, Ahmed Asim Al-Ali

Department of Prosthodontics, College of Dentistry, University of Mosul, Mosul, Iraq

ABSTRACT

Background: The additive manufacturing technology made the topology optimization technique feasible. This technique can indefinitely reduce the weight of the printed items with a promising increase in the mechanical properties of that item.

Materials and Methods: In the current experimental study, 50 samples were fabricated for a 3-point bending test. They were divided into (n = 5) as a control Group 1 free of internal geometries, (n = 15) for each of Groups 2–4, and they were subdivided into (n = 5) for each percentage of reduction per volume (10%, 15%, and 20%). Spherical, ovoid, and diamond shapes were each group's fundamental geometries, respectively. Cylindrical tunnels connected the voids in each group. Radiographic images were performed to validate the created geometries, the weight was measured, and flexural strength and modulus of elasticity were calculated. Data were analyzed by one-way ANOVA and Duncan's *post hoc* tests at $P < 0.05$.

Results: The weight results showed a significant reduction in mass. The flexural strength of Group 2 at a 10% reduction per volume had the highest mean significantly without compromising the elastic modulus. In comparison, the means of group 4 at 20% reduction showed the lowest level of toughness.

Conclusion: The weight was reduced according to the reduction percentage. The flexural strength of Group 2 at a 10% reduction showed the highest degree of toughness among all groups. The void shape and density influenced the mechanical properties tested.

Key Words: 3D printing, computer-aided design, dental prosthesis design, manufactured materials, porous coordination

Received: 06-Oct-2023
Revised: 27-Dec-2023
Accepted: 19-Feb-2024
Published: 26-Mar-2024

Address for correspondence:
Lecturer. Dr. Abdullah Jasim Mohammed,
Department of Prosthodontics, College of Dentistry, University of Mosul, Mosul, Iraq.
E-mail: abdoalla2009@uomosul.edu.iq

INTRODUCTION

The additive manufacturing method (AM) is a relatively new method for producing solid structures, including metallic removable and fixed partial dentures.[1] Although the traditional casting method has been employed to create cobalt–chromium (Co–Cr) frames for many years, it has been superseded by AM technology.[2] Metallic frameworks can be produced more simply by selective laser melting (SLM) AM technology with appropriate computer-aided design (CAD).[3-6] Topology optimization and topology modification are computational methodologies employed to generate an optimal arrangement of materials inside a designated design space, considering certain loading circumstances. The primary objective is to minimize the structure's overall weight while simultaneously satisfying other functional

Access this article online

Website: www.drj.ir
www.drjjournal.net
www.ncbi.nlm.nih.gov/pmc/journals/1480

This is an open access journal, and articles are distributed under the terms of the Creative Commons Attribution-NonCommercial-ShareAlike 4.0 License, which allows others to remix, tweak, and build upon the work non-commercially, as long as appropriate credit is given and the new creations are licensed under the identical terms.

For reprints contact: WKHLRPMedknow_reprints@wolterskluwer.com

How to cite this article: Mohammed AJ, Al-Ali AA. The influence of internally architected voids in the creation of high-strength, low-weight 3D-printed cobalt-chromium prototypes. Dent Res J 2024;21:21.

criteria.[7-9] Another benefit of the technology is that it enables the creation of finished products with virtually infinite patterns. CAD geometries and features may be manufactured using metal laser sintering (MLS) devices, including undercuts, spaces, and intricate interior geometries.[4,10,11] The topology-modified designs can be used to create hollow structures, making it possible to construct lighter things while drastically increasing productivity and reducing the quantity of powder needed during manufacturing.[12,13] Previous studies analyzed the mechanical characteristics of MLS-produced Co–Cr specimens with internal changes. They indicated that a substantial quantity of metal material could be preserved by modifying the internal geometry, production time could be decreased, and, importantly, the new internal architecture geometry yet complies with the mechanical characteristics required for the International Organization for Standardization (ISO Type 5).[14] Creating voids or modifying topology in metals with high melting points is extremely difficult, if not impossible when the conventional fabrication methods are used. Even when special chemical media and techniques are used, this can create uncontrolled shapes and sizes of the voids.[15] As an alternative, metallic objects with pores might be created by AM with no restrictions on the temperature at which they melt. In addition, the pore ratio and structure in an object constructed with AM with an interior porosity may be modified to accommodate the functionally categorized performance of design requirements.[16,17] Challis *et al*. stated that Ti6Al4V geometry optimal lattice arrangement manufactured using the SLM technique had superior rigidity and strength compared to analogous composites.[17] Takezawa *et al*. utilized topology optimization to determine the optimal lattice network geometry to reduce the performance loss caused by laser powder-removal cavities in the electron beam melting) technique.[18] Liu *et al*. discussed the fatigue properties of a CP-Ti lattice network that contains topology-optimized and rhombic cell structures manufactured by SLM.[19] Other previous studies had reported the benefits of lattice network internal geometry when compared with randomized voids distributed in the printed objects, where the lattice design can avoid local buckling of the face sheets and decrease transmitted stress under impact stresses, showing that the lattice-based structures constructed from stainless steel and SLM technique demonstrated superior rigidity, stress, and energy absorption capacity compared to unevenly shaped and distributed voids.[20-22] All aforementioned studies have emphasized the lattice-built internal structure, and its superiority in the mechanical properties improvement when compared with other voids shape, but they neglected the role of these shapes in crack propagation redirection, consequently increasing the stress needed to induce failure in the 3D-printed objects compared to the compact samples.[23,24] As a result, this study aimed to evaluate the influence of three types of internally custom-created geometric voids on the weight reduction and the mechanical characteristics of the 3D-printed Co–Cr samples. The weight, flexural bending strength, and bending modulus of elasticity of the laser-sintered Co–Cr frameworks fabricated by the direct MLS (DMLS) method was evaluated. The study hypothesis is that incorporating custom-designed voids inside the metallic denture base can reduce the 3D-printed Co–Cr prototype's weight, and enhance its mechanical properties.

MATERIALS AND METHODS

In the current experimental study, 50 samples were designed using the AutoCAD 2017 software program (AutoDesk Co., San Francisco, USA) to incorporate geometries of self-reinforced custom-designed voids inside the test samples. The samples were fabricated with Co–Cr metal powder (Adentatec, GmbH, Germany) and manufactured using the DMLS method (DMLS) technology by the laser melting machine (Riton, dual-150, Guangdong, China) with fabrication parameters as listed in Table 1. According to the American Society for Testing and Materials (ASTM standard E9) (2010), each subgroup had five samples to be tested.[25] The fabricated samples were divided into four groups. The first group (Group 1, $n = 5$) was

Table 1: Standard parameters of three-dimensional printing process with Riton dual 150 machine

Parameter	Value
Laser speed (mm/s)	1050
Laser power (W)	165
Support laser power (W)	140
Layer thickness (powder supply) (mm)	0.05
Oxygen content (%)	0.06
Building plate (mm)	150×150×110
Building direction (°)	0
Protect gas	Argon
Scan speed (mm/s)	14,000
Operating system	Windows XP
Wavelength (μm)	1064

compact without incorporating any internal design representing the control group and the second group was fabricated basically, with spherical internal voids. The third group was manufactured by incorporating ovoid voids as a basic shape. The fourth group was manufactured with diamond voids as a basic shape of the internal design. Each one of the last three groups (except for the control group) was subdivided into three subgroups ($n = 5$) according to the reduction percentage of the volume (10%, 15%, and 20%).

The samples were fabricated (1 mm thickness, 3 mm width, and 31 mm length) according to the noncasted metallic dental restoration specification of ISO standardization (22674:2016),[26] where the control group samples were printed as compact samples without an internal modification, and the rest of the samples were fabricated with the exact dimensions externally, and with internally incorporated voids. The samples were weighted to find the amount of reduction per mass of the samples using a digital balance (with 0.000 g precision; PG 503-S MonoBloc inside, Mettler Toledo Ltd, Switzerland). Then, the samples were tested using a universal testing machine (GESTER International Co., LTD, Fujian, China) with a 1.5 mm/min crosshead speed. The data gathered were subjected to the following equation to find the ultimate flexural strength (UFS):[27]

Flexural strength (σ) = $3PL/2wt^2$

Where P is the applied force value, L is the testing length from one supporting pin to the other, which is 20 mm out of the 25 mm length of the sample, w is the width of the sample, and t is the thickness of the sample.

The calculation of the flexural modulus of elasticity (apparent elastic modulus E_a) was conducted according to the following equation:[26]

Apparent elastic modulus $E_a = PL^3/4dwt^3$

Where P is the applied load, L is the length between the supporting pins = 20 mm, d is the highest deflection value, w is the width of the sample, and t is the thickness of the sample.

Incorporated internal geometries

The geometries integrated within the core of the 3-point bending samples with closed cell configuration. One of the connectors was extended to the end of the samples to achieve the enclosed cell printing efficiently to serve as a channel through which the nonsintered alloy particles can exit after the manufacturing procedure.[28] The first group was devoid of any internal geometries, where the created object was compact and used as a control group. In the second group, the incorporated geometry was spherical, where the spheres created ranged from 200 to 500 μm in diameter according to the percentage of volume reduction, and they were connected with tunnels that had ≈ 50%–75% diameter to the diameter of the sphere; also, the length of the cylindrical tunnels among the spheres was ranging from ≈ 50% to 125% to the diameter of the sphere according to the volume reduction percentage. In the third group, ovoid-shaped voids were created and arranged in transverse orientation with 200–500 μm lesser diameter and 400–1000 μm greater diameter. The tunnels also connected the ovoid voids using the lesser diameter of the oval shape as a reference, with the same connector diameter and length ratios used in the second group. In the fourth group, diamond-shaped voids were designed with symmetrical vertical and horizontal diameters of 200–500 μm, and the cylindrical tunnels connected them with the same diameter and length ratios used in the second group, which varied according to the reduction percentage. For all samples designed, the created internal geometries were located on one level in the core of the specimen. The four sides of the specimen had at least 0.5 mm thickness. In contrast, the upper and lower surfaces had a thickness range of 0.5 ± 0.05 mm according to the reduction percentage. The illustration of the designs of the four groups is shown in Figure 1.

Printing trueness tests of the topology generative modification

To validate the printing trueness of the topology modification used in the current study, the samples of groups (2–4) were imaged by digital X-ray to verify the trueness of the 3D printing of the samples using a digital dental radiographic machine (Planmeca, Helsinki, Finland). The fractographs of the three-point bending test with (1 mm × 1 mm in the X and Y directions) field in the cross section of the fractographs were subjected to microscopic analysis by material optical microscope (SLX, Optika Co., Bergamo, Italy) with magnification power (×4.5); to verify the production of hollow geometries.

To verify the changes in the surface of the final printing layer due to the presence of the hollow shapes, the surface topology of the walls of the hollow structures in the fractographs was compared to the dorsum surface (final printed layer) of the control

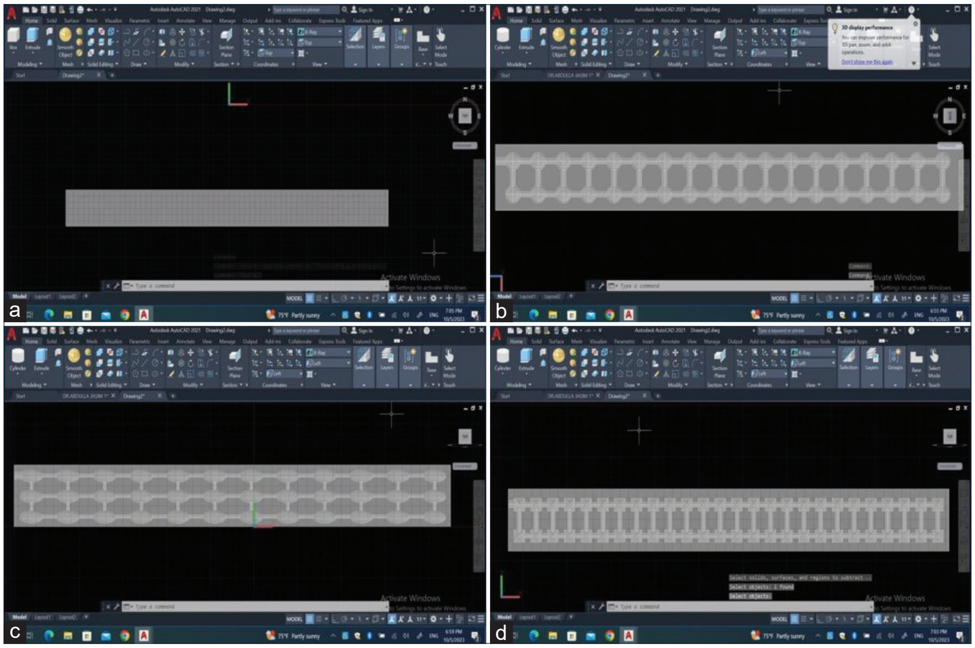

Figure 1: AutoCAD designs of the four groups. (a) Compact design of the 3-point bending test sample, (b) Sphere-based design of the 3-point bending test sample, (c) Ovoid-based design of the 3-point bending test sample, (d) Diamond-based design of the 3-point bending test sample.

group by the Atomic Force Microscope (AFM) NX7 (Park Systems Corp., Suwon, Korea), to conduct this test five samples of each group were used, where a spot on the internal wall of each basic shape used was selected with dimensions (20 µm × 20 µm) of the X and Y coordinates, the areas of eight dendritic projections within the spot were measured, and the mean values were gathered as a statistical data. The density of distribution of the dendritic projections on the surface layer was calculated per (1 mm^2) by the AFM computer program. Another test of the surface topology was conducted using a scanning electron microscope (SEM) Sigma 300 VP (Zeiss Co., Zagreb, Croatia) with (4.24 µm) imaging field. Finally, the oxide layer of the end-layer at the hollow shapes walls was compared to the end-layer of the control samples' surfaces to estimate the composition of the oxide layer in the four groups using X-ray diffraction analysis (XRD) using shine family portable device (LAN Scientific Co., Suzhou, China).

The current study was approved by (The Research Ethics Committee College of Dentistry/University of Mosul code: UoM.Dent. 23/41).

Statistical analyses

The statistical analyses were conducted using the SPSS version 17 program (SPSS Inc., Chicago, IL, USA). Multiple range tests of ANOVA and Duncan's were performed to evaluate the statistical means and significance of weight, flexural strength, and elastic modulus at a significance level of $P < 0.05$.

RESULTS

The current study theorized that one of the mechanical properties of the 3D-printed samples could be enhanced by incorporating internal geometries at a certain percentage of reduction. Subsequently, the weight would be reduced in addition to the time of printing and cost. To achieve this goal, three types of internal geometry were incorporated inside the samples to be tested. The weight, UFS (stress at rupture of the samples), and flexural modulus of elasticity were estimated at different degrees of reduction percentages.

Weight reduction results

The statistical analysis of the means and standard deviation of the weight is shown in Table 2. The results revealed that there was a significant decrease in weight for Groups 2–4 in comparison to the weight of the compact samples in Group 1 at a reduction percentage of 10% per volume, the reduction of mass at this percentage estimated about (20.4%–21.5%). Results of the weight reduction at 15% per volume showed that there was a significantly decreased weight of Groups 2–4 when compared to Group 1 compact samples; the percentage of weight reduction at this level was (26.9%–29.3%). Results of the weight reduction at a reduction of 20% per volume showed that the weight mean of Group 1 was significantly higher than those of Groups 2–4, and the samples were reduced by (31.7%–33.2%) per weight. Furthermore, results showed insignificant differences among the groups' means of weight reduction with the same reduction percentage per volume in Groups 2–4.

Flexural strength results

The mean and standard deviation of the flexural strength are shown in Figure 2. The results revealed that the UFS of Group 2 at a reduction (10%) per volume (1821.989 ± 60.103 MPa) was significantly higher than the compact samples, and the rest of the groups, followed by insignificantly different means of Group 1 UFS mean (1675.456 ± 18.360 MPa), and UFS mean of Group 2 at 15% reduction per volume (1674.364 ± 36.207 MPa). The results showed a significant declination of the UFS mean of Group 2 after a 20% reduction per volume (1465.1200 ± 42.505 MPa). The means of UFS in other groups showed significant differences at different reduction percentages of volume in Groups 3 and 4, where UFS mean Group 3 at 10% reduction (1173.262 ± 10.346 MPa), which was lower than 20% reduction of Group 2, and higher than the UFS means of the same group at 15%, and 20% reduction per volume (1128.926 ± 7.242 MPa and 996.414 ± 13.179 MPa), respectively. In Group 4, the UFS mean at a 10% reduction per volume (1131.952 ± 5.970 MPa) was insignificantly different from Group 3 at a 15% reduction per volume, the mean of UFS at 15% reduction (1043.510 ± 50.215 MPa) was significantly lower than the rest of groups at different percentages of reduction, and only significantly higher than UFS mean of the same group at 20% reduction per volume (928.040 ± 76.678 MPa).

Table 2: The means and standard deviation of the weighted mass of the four groups

Groups	Reduction % per volume	*n*	Weight (g)±SD
Group 1	-	5	0.8895±0.04184^{a}
Group 2	10	5	0.7070±0.00982^{b}
	15	5	0.6495±0.01843^{c}
	20	5	0.5970±0.00851^{d}
Group 3	10	5	0.6978±0.00497^{b}
	15	5	0.6286±0.07317^{c}
	20	5	0.6076±0.01853^{d}
Group 4	10	5	0.7047±0.00623^{b}
	15	5	0.6501±0.02539^{c}
	20	5	0.5930±0.00872^{d}
Significance			0.00

Where SD is the standard deviation, means labeled with different letters indicate significant differences

Elastic modulus results

The elastic modulus or modulus of elasticity is the value that represents a change in the material within the elastic limits; in other words, it is the degree of elastic deformation of the material when it is under specific stresses that do not reach the proportional limits of the material. The modulus of elasticity value is highly important because it indicates the material's stiffness. Subsequently, higher elastic modulus values mean that the major connectors of the removable partial dentures can distribute stresses induced in the oral cavity before it deforms. The elastic modulus results (mean and standard deviation) are shown in Figure 3. The results revealed that there were insignificant differences among the means of the elastic modulus in the

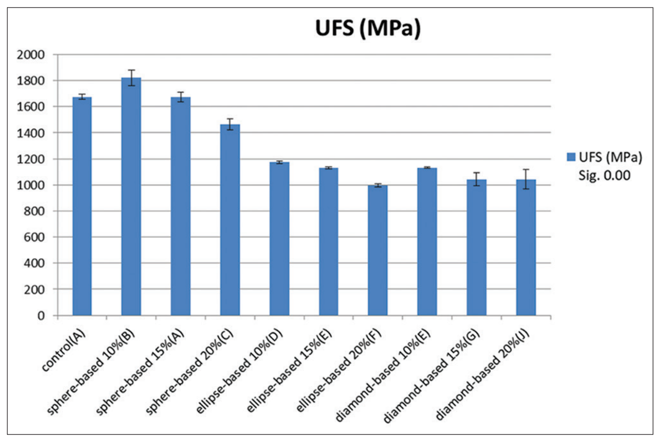

Figure 2: Bar graph of the statistical analysis of the ultimate flexural strength mean and standard deviation. Bar names with identical letters indicate insignificant differences. UFS: Ultimate flexural strength.

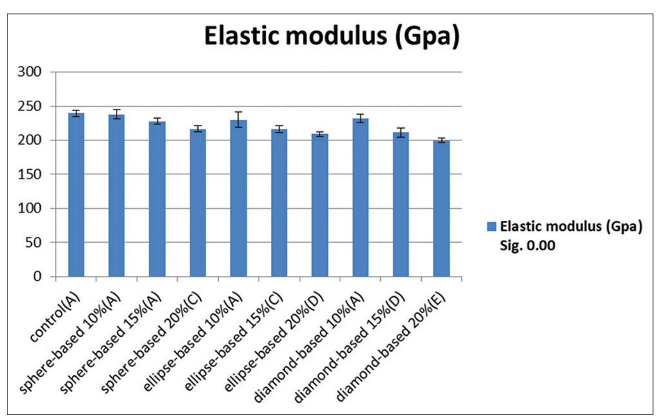

Figure 3: Bar graph of the statistical analysis of the elastic modulus mean and standard deviation. Bar names with identical letters indicate insignificant differences.

four groups (239.632 ± 4.310, 238.232 ± 7.016, 233.478 ± 8.528, and 238.158 ± 6.220) GPa, respectively, at 10% reduction per volume. The results showed a declination in the means of the elastic modulus of groups 2–4 at a 15% reduction per volume, and a further significant declination occurred at a 20% reduction per volume. In Group 2, the mean at a 15% reduction (234.140 ± 4.425 GPa) was insignificantly lower than that at a 10% reduction but still significantly higher than a 20% reduction (216.848 ± 4.838 GPa) in the same group. The mean of elastic modulus in the Group 3 at 15% reduction (216.142 ± 5.1387) showed an insignificant difference with that of the Group 2 at 20% per volume reduction. The mean of the modulus of elasticity of Group 3 at 20% (209.244 ± 3.474 GPa) had a significantly lower value than that at 15% of the same group and an insignificant difference from that of Group 4 (211.422 ± 6.3519 GPa) at 15% reduction, which was higher significantly than that of the same group (199.518 ± 3.348 GPa) at 20% reduction.

Printing trueness test results

The radiographic imaging was conducted to validate the printing trueness of the 3D printing of the integrated hollow structures. Radiographic imaging revealed consistent printing of the proposed design of the three types of geometries apart from neglected overhangs of the 3D printing process, as illustrated in Figure 4.

The visual inspection of the microscopic images of the geometric shapes revealed an acceptable production level of the basic hollow shapes by the DMLS method of AM, where the basic hollow geometries (listed in Figure 5 column A) were successfully printed with higher accuracy of the sphere-based and ellipse-based shapes when compared to the diamond-based geometry as illustrated in Figure 5 Column B.

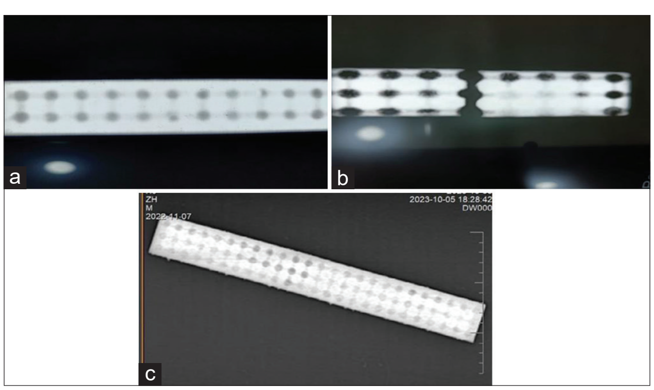

Figure 4: Radiographic image of the three integrated designs. (a) sphere-based (b) ovoid-based (c) diamond-based geometries.

The atomic force microscopy of the walls of the hollow shapes revealed that there was a dendritic surface texture for the surface of the sample and the walls of the hollow shapes, indicating insignificant changes because all the samples were fabricated with the same method of printing (DMLS) and the same type of the alloy powder as shown in Figure 5 Column C.

The statistical results of the surface roughness gathered from the AFM demonstrated insignificant differences among the control surface of the samples and the walls of the printed geometries; the mean and standard deviation of the subgroups of groups 1–4 and the sample surface are listed in Table 3.

The SEM images of the four groups illustrated an insignificant difference among the groups where the surface layer appeared with relatively round dendritic surface topology with no apparent alteration of the surface contents or particle distribution, as shown in Figure 5 Column D. The graphs of the XRD test estimated the occurrence of elements in the oxide layer of amplitude and width of the generated wave. The results illustrated that the oxide layer of the four groups was composed of four main elements (carbon, nickel, chromium, and oxygen) and trace elements (sulfur, silicon, cobalt, and alcium), as shown in Figure 6.

DISCUSSION

This investigation analyzed the effect of internal structural design on the mechanical properties of DMLS-fabricated Co–Cr specimens. The results revealed that the internal structural design with sphere-based hollow structures at 10% volumetric reduction reduced the specimens' weight significantly and had no effect on their modulus of elasticity. Simultaneously, there was a significantly increased flexural strength of the same reduction percentage of the same group compared to the compact samples of the control group. Therefore, the hypothesis was accepted for the mass reduction, flexural strength, and elastic modulus parameters.

Weighting test of the 3D-printed samples

Results revealed a significant reduction in weighted samples compared to the compact samples. Furthermore, the weights of the tested samples

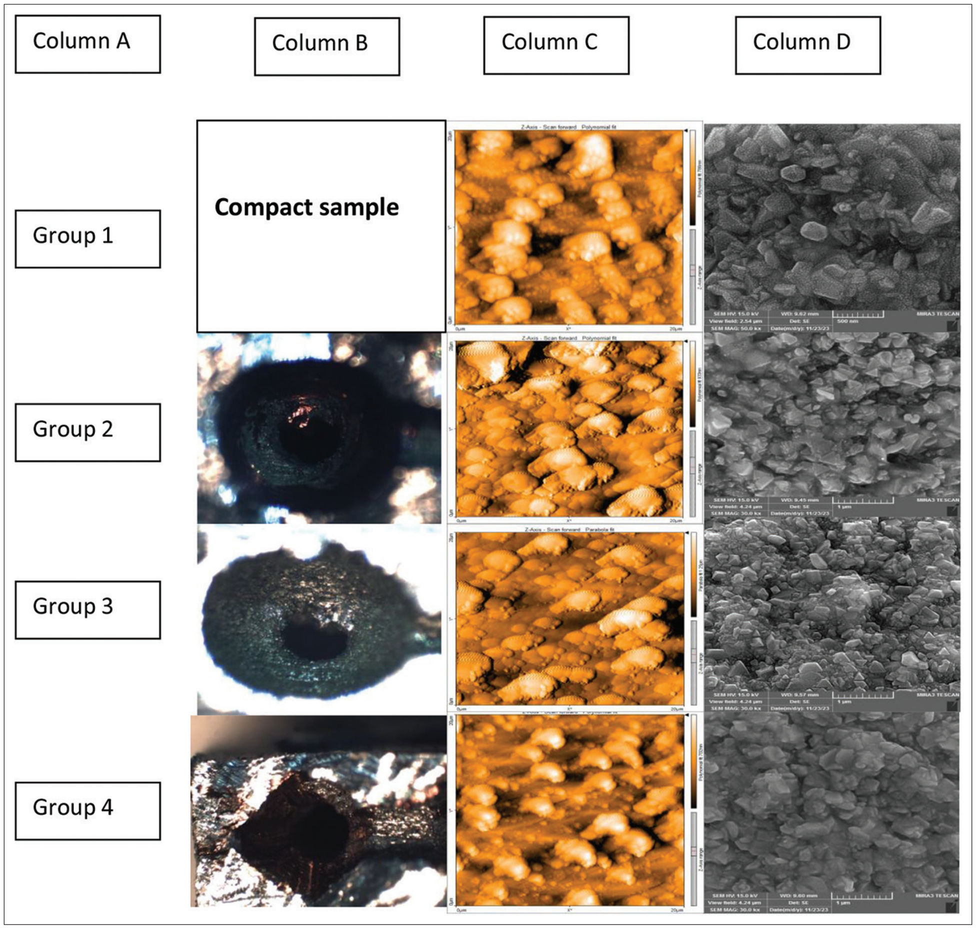

Figure 5: Microscopic images, scanning electron microscope (SEM) images, and atomic force microscope (AFM) images of the groups. (Column A) The name of the group, (Column B) The microscopic image of the basic hollow shape, (Column C) The SEM images of the surface layer (4.24 μm), (Column D) The AFM surface images (20 μm × 20 μm).

Table 3: The mean and standard deviation of the dendritic particle's areas and density of distribution were measured by the AMF test

Groups	Reduction % per volume	*n*	Area of particles nm²±SD	Density of particles/ mm²±SD
Group 1	-	5	52,177.0±3613.979(*)	931,384.4±12,640.462(**)
Group 2	10	5	52,417.6±3927.531(*)	928,783.8±16,164.454(**)
	15	5	52,261.4±3590.938(*)	928,886.2±11,926.467(**)
	20	5	52,450.0±4590.705(*)	934,968.4±19,345.894(**)
Group 3	10	5	51,716.2±3972.080(*)	928,892.8±11,680.769(**)
	15	5	52,666.8±3113.973(*)	936,062.8±13,408.696(**)
	20	5	51,206.6±3480.939(*)	928,156.2±16,185.671(**)
Group 4	10	5	52,890.4±3887.300(*)	936,065.8±19,368.564(**)
	15	5	52,331.6±3120.045(*)	934,067.8±21,051.855(**)
	20	5	51,941.6±4182.708(*)	938,792.0±17,021.545(**)
Significance			1.00	0.970

Where SD is the standard deviation, means labeled with identical symbols indicate insignificant differences. AMF tested field: (20×20μm)

were significantly different at different reduction percentages. The internally integrated micro-voids can decrease the mass of the additively manufactured objects due to the apparent reduction in density, consequently reducing the cost and period of the printing procedure.[13,28,29] These results are consistent with previous studies that confirmed a significant mass reduction when hollow structures are incorporated inside the printed object relative to the reduction in density of the item.[30,31]

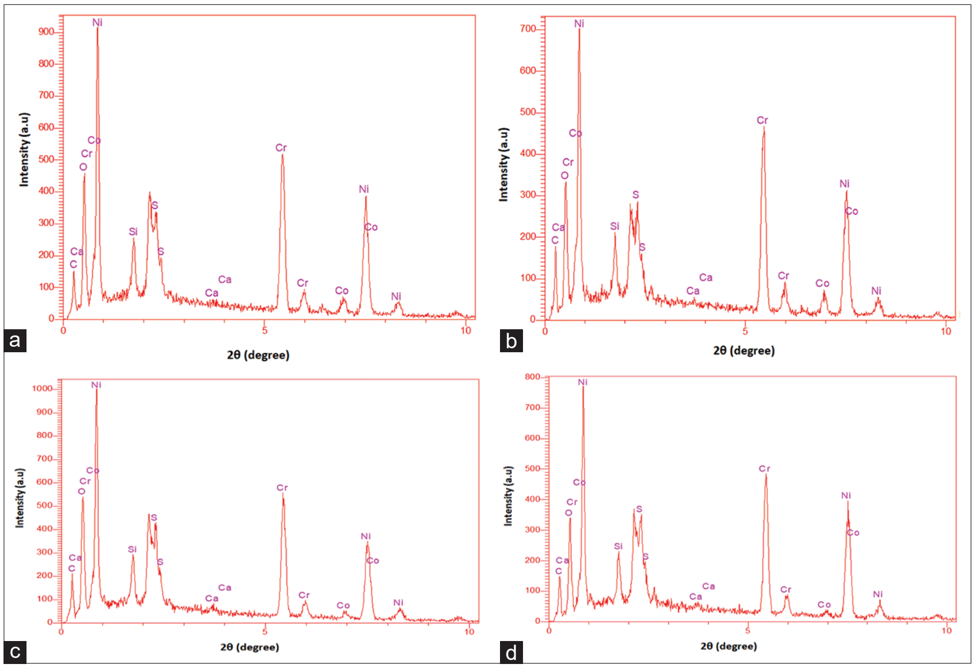

Figure 6: X-ray diffraction analysis of the oxide layer of the samples. (a) The control group surface oxide layer, (b) The sphere-based group oxide layer, (c) The ovoid-based group oxide layer, (d) The diamond-based group oxide layer.

Flexural strength of the 3D-printed samples

Results of the flexural strength revealed that the flexural strength was increased in the Group 2, where a sphere-based hollow structure was created at a 10% reduction per volume. The rigidity of the objects decreased with increased volume reduction and different shapes of the internal geometries. The results presented in this paper demonstrated that designed spherical voids offer a substantial potential for strengthening additively manufactured components and frameworks. An increase in fracture resistance, particularly considering that this improvement resulted from a minor geometrical modification, possibly because of crack arrest and termination, whereas the corresponding conventional geometries fractured catastrophically at relatively modest driving forces, the modified geometries resisted more external stresses. This characteristic of crack arrest may be a crucial component of the designing strategy, permitting secure, measurable deformation of an object before its catastrophic breakdown.[29-31] Adding micro-voids to a topological strengthening of the materials can offer another freedom level in object design. The capacity to add designs broadens the design characteristics for targeted strengthening. It enables different approaches for targeted strengthening with designed voids, and this would be useful in predicting the directions of crack growth, creating nonlinear propagation of the fracture.[32,33] The planes of voids could generate directed interfaces to control the crack growth and enhance the strength of the material.[34] The increased values of the flexural strength in Group 2 at a 10% reduction per volume, without compromising the elastic modulus values, and the insignificant difference of the same group at a 15% reduction per volume indicate that the spheres designed were capable of absorbing the stress-energy, and, distribute this energy horizontally, in other words, the crack growth was inhibited by the presence of angle-free internal void, where the stress-induced could not concentrate at any point at the metallic shell surrounding the voids. Because its percolated boundary has a rounder junction, which induces less stress concentration and increases resistance to bending deformation, the spherical structure has noticeably higher stiffness and strength due to the higher resistance to bending deformations compared to the compact samples. This effect of voids could also be increased because the tunnels connecting the voids used in the current study may further redirect the crack growth in a horizontal direction. The crack propagation could also be dissipated and split into more than one division by the presence of a sphere angle-free metallic shell around the spherical micro-voids.[35,36] Furthermore, the algorithmic rise of the internal gaseous pressure in a spherical void in solid objects could contribute to higher levels of flexural strength.[37,38] The results of the current study were totally in agreement with previous studies' findings.[36,39] It is partially consistent with previous studies that reported a relatively superior flexural strength induced by better energy absorption after incorporating internally arranged voids.[20,21,40,41] The current study showed a significant difference in flexural strength among groups 2–4 with different geometries. The difference could be the result that these shapes have different absorption capacities of the external stresses induced in the three-point bending test, where spherical shapes are devoid of angles that act as a center for stress concentration in the case of Group 4 and long linear courses that are perpendicular to the external force applied in case of Group 3, where the ovoid shapes could act in the same way of ellipsoidal shapes in other studies.[42] These results agree with other studies that reported significant differences among different internal geometries incorporated inside the 3D-printed objects due to different energy absorption levels and distribution.[15,35,42] The current results were inconsistent with other studies that reported insignificant differences among different geometries or better absorption of geometries designed with certain angular architects.[43] The results also revealed that there was a gradual regression in the values of flexural strength and elastic modulus, starting from Group 2 at a 10% reduction per volume, which had the highest means of flexural strength among other groups and reduction ratio, to the least means the flexural strength of Group 4 at 20% reduction per volume. These results indicate that the regression is the factor of reduced density of the printed objects, where the reduced density corresponded to larger voids per volume, which act as focal spots for crack growth. Furthermore, the density of the topologically modified parts plays an important role in flexural strength where at specific high levels of density (mass) reduction, the hollow shapes can reduce the flexural strength of the printed objects so that the density reduction is a critical value and can counteract the intended purpose of its integration at a certain level.[15,29]

Elastic modulus

The findings demonstrated that the average elastic modulus gradually decreased in relation to a gradual decrease in the strength and an increase in the reduction percentage within each subgroup. Specifically, the highest mean elastic modulus was observed in the sphere-based structure with a 10% volume reduction. Conversely, the ellipse-based and diamond-based geometries with a 20% volume reduction exhibited the lowest mean elastic modulus. These results indicate a clear correlation between the gradual decrease in mean elastic modulus and the gradual decrease in flexural strength, particularly when the strain of the measured objects is nearly identical. This occurrence is typically characterized by a high degree of brittleness and significantly reduced flexibility. These properties can be attributed to the lower grain dislocation observed in the tested samples.

Furthermore, the samples were printed in a transverse orientation relative to the force exerted throughout the testing process. This further contributes to the increased deflection values of groups with lower stiffness, where the deflection values are inversely proportional to the modulus of elasticity.[41,43,44]

Printing trueness tests

The radiographs of the 3-point bending samples illustrated that the printing of the proposed hollow structures was proved by the presence of the intended geometries inside the test samples. In the current study, the AutoCAD program was used for designing the samples, and the Materialise Magics program was used as a slicing program. These two programs can properly transfer precise dimensions as digital information to the 3D-printing machine program to produce printed items with high precision and accuracy of the proposed dimensions.[29,45-47]

The analysis of the fractographs of the printed hollow shapes indicated that all geometries were efficiently created using the DMLS technology. Furthermore, examining the cross-sections of the three geometries revealed that the geometrical structures with round forms in the sphere and ellipse were produced satisfactorily, with no or minimal leftover residues. On the other hand, the diamond-shaped objects showed more significant variations, particularly in the upper and lower regions near the sharp inclinations. This suggests that hollow shapes with sharp angles may have lower print quality compared to shapes with circular bases and tops. These findings show that the parameters employed in the DMLS procedure and the selected relocation position were suitable for producing the hollow components.[47,48] Atomic force microscopy microscopic images, SEM images, and XRD test results showed a dendritic surface production of the printing procedure, which was insignificantly different qualitatively and quantitatively among the tested surfaces of the control samples. The walls of the hollow shapes are probably because of the same printing method (DMLS) and the same powder alloy used to fabricate all samples, and especially there was no heat treatment involved in the current study.[2,7,11,48,49]

One of the study limits is that the real-time printing of each specimen could not be estimated. Therefore, the statistical results were not correlated to the printing time factor; also, the thickness variation of the samples was not considered in the current study. Clinical evaluation of the results gathered in this study should be conducted before applying the current research findings.

CONCLUSIONS

Within the limitations of the current experimental work, we can state that the graded volumetric reduction significantly reduced the mass of the printed objects, producing items with less density at all levels (10%, 15%, and 20%) of reduction per volume used in this study. Incorporating a sphere-based hollow structure at a 10% reduction per volume can reduce the weight and increase the flexural strength of the 3D printed objects without compromising the elastic modulus property with evident printing quality and quantity of the hollow structures.

Financial support and sponsorship
The research is self-funded.

Conflicts of interest
The authors of this manuscript declare that they have no conflicts of interest, real or perceived, financial or non-financial in this article.

REFERENCES

1. Önöral Ö, Ulusoy M, Seker E, Etikan İ. Influence of repeated firings on marginal, axial, axio-occlusal, and occlusal fit of metal-ceramic restorations fabricated with different techniques. J Prosthet Dent 2018;120:415-20.
2. Ucar Y, Ekren O. Effect of layered manufacturing techniques, alloy powders, and layer thickness on mechanical properties of Co-Cr dental alloys. J Prosthet Dent 2018;120:762-70.
3. Obeidi MA. Metal additive manufacturing by laser-powder bed fusion: Guidelines for process optimisation. Results Eng 2022;15:100473.
4. van Noort R. The future of dental devices is digital. Dent Mater 2012;28:3-12.
5. Shoujin Z, Qirui W, Jianhua Y. Mechanical properties of 316L stainless steel porous structure formed by selective laser melting. Infrared and Laser Engineering 2020;49(8): 20190523.
6. Guo N, Leu MC. Additive manufacturing: Technology, applications and research needs. Front Mech Eng 2013;8:215-43.
7. Mahato V, Obeidi MA, Brabazon D, Cunningham P. Detecting voids in 3D printing using melt pool time series data. J Intell Manuf 2022;33: 845-852.
8. Sohrabpoor H, Mousavian RT, O'Halloran S, Benyounis KY, Baraheni M, Obeidi MA, *et al*. Experimental and empirical model analysis of microsurface texturing on 316 L press-fit joints fabricated by selective laser melting. Int J Adv Manuf Technol 2020;108:2687-99.
9. Ramya A, Vanapalli SL. 3D printing technologies in various applications. Int J Mech Eng Technol 2016;7:396-409.
10. Farjood E, Vojdani M, Torabi K, Khaledi AA. Marginal and internal fit of metal copings fabricated with rapid prototyping and conventional waxing. J Prosthet Dent 2017;117:164-70.
11. Takaichi A, Suyalatu, Nakamoto T, Joko N, Nomura N, Tsutsumi Y, Migita S, Doi H, Kurosu S, Chiba A, Wakabayashi N, Igarashi Y, Hanawa T. Microstructures and mechanical properties of Co-29Cr-6Mo alloy fabricated by selective laser melting process for dental applications. J Mech Behav Biomed Mater 2013;21:67-76.
12. Khorsandi D, Fahimipour A, Abasian P, Saber SS, Seyedi M, Ghanavati S, Ahmad A, De Stephanis A, Taghavinezhaddilami F, Leonova A, Mohammadinejad J, Shabani M, Mazzolai B, Mattoli B, Tay FR., Makvandi P. 3D and 4D printing in dentistry and maxillofacial surgery: Printing techniques, materials, and applications. Acta Biomater 2021;122:26-49.
13. Ekren O, Kocak EF, Ucar Y. Effect of internal design changes on the mechanical properties of laser-sintered cobalt-chromium specimens. J Prosthet Dent 2023;129:508-12.
14. Ryan G, Pandit A, Apatsidis DP. Fabrication methods of porous metals for use in orthopaedic applications. Biomaterials 2006;27:2651-70.
15. Zhang P, Toman J, Yu Y, Biyikli E, Kirca M, Chmielus M, *et al*. Efficient design-optimization of variable-density hexagonal cellular structure by additive manufacturing: Theory and validation. J Manuf Sci Eng 2015;137(2):0210041-0210048.
16. Xu Y, Li T, Cao X, Tan Y, Luo P. Compressive properties of 316L stainless steel topology-optimized lattice structures fabricated by selective laser melting. Adv Eng Mater 2021;23(3): 2000957.
17. Challis VJ, Xu X, Zhang LC, Roberts AP, Grotowski JF, Sercombe TB. High specific strength and stiffness structures produced using selective laser melting. Mater Des 2014;63:783-8.
18. Takezawa A, Koizumi Y, Kobashi M. High-stiffness and strength porous maraging steel via topology optimization and selective laser melting. Addit Manuf 2017;18:194-202.
19. Liu YJ, Ren DC, Li SJ, Wang H, Zhang LC, Sercombe TB. Enhanced fatigue characteristics of a topology-optimized porous titanium structure produced by selective laser melting. Addit Manuf 2020;32: 101060.
20. Zhang L, Feih S, Daynes S, Chang S, Wang MY, Wei J, Lu W *et al*. Energy absorption characteristics of metallic triply periodic minimal surface sheet structures under compressive loading. Addit Manuf 2018;23:505-15.
21. Al-Saedi DS, Masood SH, Faizan-Ur-Rab M, Alomarah A, Ponnusamy P. Mechanical properties and energy absorption

capability of functionally graded F2BCC lattice fabricated by SLM. Mater Des 2018;144:32-44.
22. Sukiman B, Karim IJ, Abbas MF. Analysis the effect of internal geometry on the mechanical properties of acrylonitril butadiene styrene (ABS) materials prepared using 3D printing. E3S Conf. ICST 2021;328:3-8.
23. Lee SC, Choi CS. An analytical study on the impact of hollow shapes in bi-axial hollow slabs. Europe ;2010;30(100):1729-1736.
24. Galeta T, Raos P, Stojšić J, Pakši I. Influence of structure on mechanical properties of 3D printed objects. Procedia Eng 2016;149:100-4.
25. American Society for Testing and Materials (ASTM) E8/E8M standard test methods for tension testing of metallic materials 1. Annu B ASTM Stand 4. 2010;(C):1–27.
26. International Standard Organization. ISO Standardization for Metallic Materials For Fixed and Removable Restorations and Appliances; Stand. 22674.2016;(E):1-36.
27. Poonacha V, Poonacha S, Salagundi B, Rupesh PL, Raghavan R. *In vitro* comparison of flexural strength and elastic modulus of three provisional crown materials used in fixed prosthodontics. J Clin Exp Dent 2013;5:e212-7.
28. Xiong Y, Yao S, Zhao ZL, Xie YM. A new approach to eliminating enclosed voids in topology optimization for additive manufacturing. Addit Manuf 2020;32:101006.
29. Okano H, Tasaka A, Matsunaga S, Kasahara M, Wadachi J, Hattori M, Abe S, Yamashita S. Effects of hollow structures added by selective laser sintering on the mechanical properties of Co-Cr alloy. J Prosthodont Res 2023;67:460-7.
30. Kocak EF, Ekren O, Ucar Y. Effect of internal design modification on the mechanical properties of laser sintered cobalt-chromium multi-unit metal-ceramic frameworks. J Prosthodont 2022;31:766-70.
31. Chiu LN, Rolfe B, Wu X, Yan W. Effect of stiffness anisotropy on topology optimisation of additively manufactured structures. Eng Struct 2018;171:842-8.
32. Li L, Khandelwal K. Design of fracture resistant energy absorbing structures using elastoplastic topology optimization. Struct Multidiscip Optim 2017;56:1447-75.
33. Kang Z, Liu P, Li M. Topology optimization considering fracture mechanics behaviors at specified locations. Struct Multidiscip Optim 2017;55:1847-64.
34. Andersons J, König M. Dependence of fracture toughness of composite laminates on interface ply orientations and delamination growth direction. Compos Sci Technol 2004;64:2139-52.
35. Al-Ketan O, Rowshan R, Palazotto AN, Abu Al-Rub RK. On mechanical properties of cellular steel solids with shell-like periodic architectures fabricated by selective laser sintering. J Eng Mater Technol 2019;141:21009.
36. Conway KM, Kunka C, White BC, Pataky GJ, Boyce BL. Increasing fracture toughness via architected porosity. Mater Des 2021;205:109696.
37. MacKenzie JK. The elastic constants of a solid containing spherical holes. Proc Phys Soc Sect B 1950;63:2-11.
38. Lynch ME, Mordasky M, Cheng L, To A. Design, testing, and mechanical behavior of additively manufactured casing with optimized lattice structure. Addit Manuf 2018;22:462-71.
39. Jin QY, Yu JH, Ha KS, Lee WJ, Park SH. Multi-dimensional lattices design for ultrahigh specific strength metallic structure in additive manufacturing. Mater Des 2021;201:109479.
40. 42 Zhao J, Zhang M, Zhu Y, Li X, Wang L, Hu J. A novel optimization design method of additive manufacturing oriented porous structures and experimental validation. Mater Des 2019;163:107550.
41. Etter T, Kunze K, Geiger F, Meidani H. Reduction in Mechanical Anisotropy Through High Temperature Heat Treatment of Hastelloy X Processed by Selective Laser Melting (SLM). IOP Conf. Ser.: Mater. Sci. Eng. 2015. 82: 12097.
42. Hyde A, He J, Cui X, Lua J, Liu L. Effects of microvoids on strength of unidirectional fiber-reinforced composite materials. Compos Part B Eng 2020;187:107844.
43. Geiger F, Kunze K, Etter T. Tailoring the texture of IN738LC processed by selective laser melting (SLM) by specific scanning strategies. Mater Sci Eng A 2016;661:240-6.
44. Pellizzari M, Jam A, Tschon M, Fini M, Lora C, Benedetti M. A 3D-printed ultra-low young's modulus β-Ti alloy for biomedical applications. Materials (Basel) 2020;13:2792.
45. Orme ME, Gschweitl M, Ferrari M, Madera I, Mouriaux F. Designing for additive manufacturing: Lightweighting through topology optimization enables lunar spacecraft. J Mech Des Trans ASME 2017;139(10):100905.
46. Koch C, Georgieva K, Kasireddy V, Akinci B, Fieguth P. A review on computer vision based defect detection and condition assessment of concrete and asphalt civil infrastructure. Adv Eng Inform 2015;29:196-210.
47. Hällgren S, Pejryd L, Ekengren J. 3D data export for additive manufacturing-improving geometric accuracy. Procedia Cirp 2016;50:518-23.
48. Song J, Wang Y, Zhou W, Fan R, Yu B, Lu Y, Li L. Topology optimization-guided lattice composites and their mechanical characterizations. Compos Part B Eng 2019;160:402-11.
49. Maconachie T, Leary M, Lozanovski B, Zhang X, Qian M, Faruque O, Brandt M.SLM lattice structures: Properties, performance, applications and challenges. Mater Des. 2019;183:108137.